Emergence of Strong Exchange Interaction in the Actinide Series: The Driving Force for Magnetic Stabilization of Curium

K. T. Moore,[1,*,†] G. van der Laan,[2] R. G. Haire,[3] M. A. Wall,[1] A. J. Schwartz,[1] and P. Söderlind[1]

[1]*Lawrence Livermore National Laboratory, Livermore, California 94550, USA*
[2]*Magnetic Spectroscopy Group, Daresbury Laboratory, Warrington WA4 4AD, United Kingdom*
[3]*Oak Ridge National Laboratory, Mississippi-6375, Oak Ridge, Tennessee 37831, USA*
(Received 9 February 2007; published 5 June 2007)

Using electron energy-loss spectroscopy, many-electron atomic spectral calculations, and density functional theory, we show that angular-momentum coupling in the $5f$ states plays a decisive role in the formation of the magnetic moment in Cm metal. The $5f$ states of Cm in intermediate coupling are strongly shifted towards the *LS* coupling limit due to exchange interaction, unlike most actinide elements where the effective spin-orbit interaction prevails. Hund's rule coupling is the key to producing the large spin polarization that dictates the newly found crystal structure of Cm under pressure.

Magnetic stabilization of crystal structures is rare and intriguing. In general, the driving force for magnetism is the exchange interaction that quantum-mechanically originates from the Pauli exclusion principle, in combination with electrostatic repulsion. In some metals, the magnetic interaction energy is sufficiently large to influence the crystal structure. Examples are manganese, iron, and cobalt where appreciable exchange interaction creates a strong magnetic moment, which in turn dictates one or more crystallographic phases [1–3]. Recently, the list of metals with known magnetically stabilized crystal structures was extended to include a heavy actinide element.

During a contemporary surge in actinide condensed-matter physics [4–11], curium was found to have a phase induced by magnetism. In a diamond-anvil-cell study [12], Cm was pressurized up to ∼100 GPa, causing the metal to undergo transformations between five different crystal structures, Cm I through Cm V. *Ab initio* calculations showed that the magnetic correlations in antiferromagnetic (AF) Cm play a crucial role in determining the crystal structures observed and that spin polarization of the $5f$ electrons is needed to achieve the correct sequence of phases during compression [12]. The calculations also showed that Cm III, which is monoclinic with the space group $C2/c$, could *not be stabilized* when spin polarization was neglected.

The $3d$ transition metals are an example where appreciable exchange interaction occurs, resulting in magnetism in some of the heavier metals in the series. However, the actinide metals exhibit a pronounced effective spin-orbit interaction of the $5f$ states due to strong relativistic effects, and this produces a considerable energy splitting and little mixing between the $5f_{5/2}$ and $5f_{7/2}$ levels [13]. Presently, there is no experimental evidence in the actinide series of the strong exchange interaction required to magnetically stabilize a metallic phase. What mechanism then produces the strong spin polarization in Cm, which in turn is responsible for the formation of the Cm III phase?

Here, we investigate the electronic and magnetic structure of Cm using electron energy-loss spectroscopy (EELS) in a transmission electron microscope (TEM), many-electron atomic calculations and density functional theory (DFT). We show that for Cm the $5f$ states in intermediate coupling are strongly shifted towards the *LS* coupling limit, unlike the lighter actinide metals that exhibit a strong effective spin-orbit interaction [13]. This so-called Hund's rule coupling in Cm is due to exchange interaction, and is the mechanism stabilizing Cm III. Experimentally, we examine the room-pressure phase, Cm I, but the observed results are meaningful for Cm II and III as well. EELS experiments in the TEM [13], theoretical x-ray absorption spectra [14–16], and DFT calculations [10,17] were performed in a similar fashion to the references cited.

To date, absorption-type experiments have not been performed on Am or Cm, leaving their unoccupied electronic structure unmeasured. Here, the $N_{4,5}$ EELS spectra for Am and Cm metal are shown in Fig. 1(a). The Am spectrum displays a strong N_5 ($4d_{5/2} \rightarrow 5f_{5/2,7/2}$) peak, but a very small N_4 ($4d_{3/2} \rightarrow 5f_{5/2}$) peak, while for Cm the N_5 and N_4 peaks are more equal in intensity. Using the experimentally measured branching ratio from the EELS spectra, atomic spectral calculations and sum-rule analysis, we can examine the transitions in detail. The branching ratio $B = I(N_5)/[I(N_5) + I(N_4)]$ was obtained as described in Refs. [15,16], where $I(N_5)$ and $I(N_4)$ are the integrated intensity of the N_5 and N_4 peaks, respectively. Sum-rule analysis was then performed using the experimental branching ratios, yielding the values of the spin-orbit interaction per hole [18]. For the f shell, the expectation value of the angular part of the spin-orbit parameter is $\langle w^{110} \rangle = 2/3 \langle l \cdot s \rangle = n_{7/2} - 4/3 n_{5/2}$, where $n_{7/2}$ and $n_{5/2}$ are the electron occupation numbers for the angular-momentum levels $j = 7/2$ and $5/2$ [15]. Thus, $\langle w^{110} \rangle$ reveals the proper angular-momentum coupling scheme for a given material. For the $d \rightarrow f$ transition, the sum
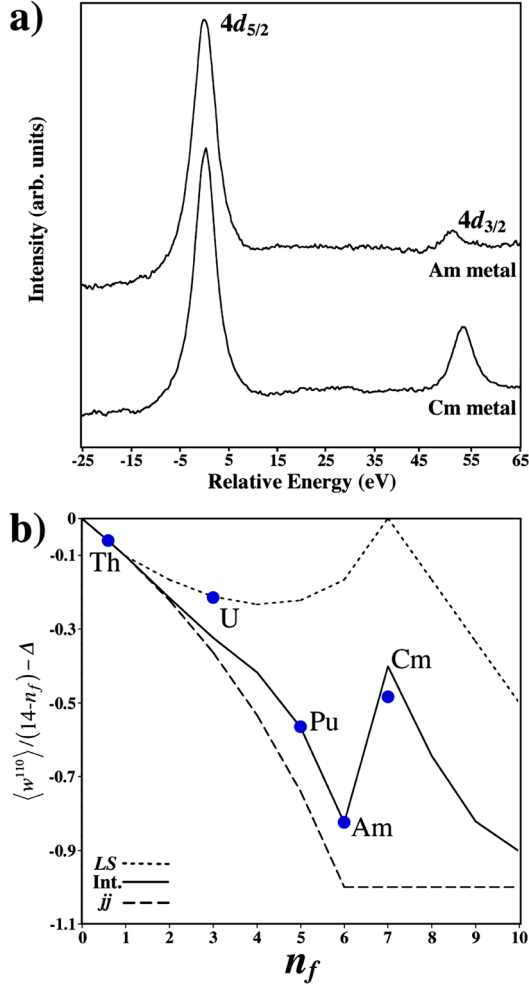
FIG. 1 (color online). (a) The $N_{4,5}$ EELS spectra of Am and Cm metal acquired in a TEM. (b) A plot of $\langle w^{110}\rangle/(14-n)-\Delta$ as a function of the number of $5f$ electrons (n_f). The three theoretical angular momentum coupling schemes are shown: LS, jj, and intermediate. Data from the experimentally measured branching ratios of each metal are indicated by points.

rule gives the spin-orbit interaction per hole as

$$\frac{\langle w^{110}\rangle}{14-n_f}-\Delta=-\frac{5}{2}\left(B-\frac{3}{5}\right),\qquad(1)$$

where B is the measured branching ratio for the experimental EELS spectra, n_f is the number of electrons in the f

shell, and Δ represents the small correction term for the sum rule that is calculated using Cowan's relativistic Hartree-Fock code [14].

The results of the spin-orbit analysis for the $N_{4,5}$ EELS spectra are plotted as points in Fig. 1(b). In addition to the present Am and Cm results, the results for Th, U, and Pu from Ref. [16] are plotted for completeness. (Pu, Am and Cm values are given in Table I.) The number of $5f$ electrons n_f for each metal is obtained from literature, where Th = 0.6, U = 3, Pu = 5, Am = 6, and Cm = 7 [19]. In addition to the EELS data, the results for LS, jj and intermediate coupling of the angular momenta, as given by atomic calculations, are plotted against the number of $5f$ electrons as a short-dashed line, long-dashed line, and solid line, respectively. Examining all the data in Fig. 1(b), it is clear that the $5f$ states of Am metal show an intermediate coupling mechanism that is close to the jj limit, meaning the majority of the six $5f$ electrons are in the $j = 5/2$ manifold. The sum-rule results for Am can in fact be understood directly from their EELS spectra in Fig. 1(a), since there is only a very small N_4 ($4d_{3/2}$) peak. Selection rules govern that a $d_{3/2}$ electron can only be excited into the $f_{5/2}$ level, and since this level is almost full, being only able to holds six electrons, there is almost no transition. The branching ratio and sum-rule analysis of Cm show it too exhibits an intermediate coupling mechanism, but in this case, it is much closer to the LS limit, as illustrated in Fig. 1(b). This results in a larger intensity of the N_4 peak, relative to the N_5 peak, as seen in the EELS spectrum in Fig. 1(a).

The physical origin of the abrupt and striking change in expectation value in Fig. 1(b) is caused by a transition from optimal spin-orbit stabilization to optimal exchange interaction stabilization. jj coupling prefers all the electrons to be in the $f_{5/2}$ level, which can hold no more than six. The maximal energy gain in jj coupling is therefore obtained for Am f^6, since the $f_{5/2}$ level is filled. However, for Cm f^7, at least one electron will be relegated to the $f_{7/2}$ level. The f^7 configuration has the maximal energy stabilization due to the exchange interaction, with all spins parallel in the half-filled shell, and this can only be achieved in LS coupling. Thus, the large changes observed in the electronic and magnetic properties of the actinides at Cm are due to this transition from optimal spin-orbit stabilization for f^6 to optimal exchange interaction stabilization for f^7.

TABLE I. The number of f electrons (n_f), the measured branching ratio, B, of the $N_{4,5}$ EELS spectra, and the expectation value of the $5f$ spin-orbit interaction per hole, $\langle w^{110}\rangle/(14-n_f)$, obtained using Eq. (1) for Pu (Ref. [16]), Am and Cm metal (current work). The sum rule requires a small correction factor, which is $\Delta = 0.000$, 0.005, and 0.015 for $n = 5$, 6, and 7, respectively. The electron occupation numbers of the $f_{5/2}$ and $f_{7/2}$ levels are obtained by solving $\langle w^{110}\rangle = n_{7/2} - 4/3 n_{5/2}$ and $n_f = n_{7/2} + n_{5/2}$.

Metal	n_f	Branching ratio (B)	$\langle w^{110}\rangle/(14-n_f)-\Delta$	$n_{5/2}$	$n_{7/2}$
Pu	5	0.826 (010)	−0.565(025)	4.32	0.67
Am	6	0.930 (005)	−0.830(013)	5.38	0.62
Cm	7	0.794 (003)	−0.485(008)	4.41	2.59

In all cases, the spin-orbit and exchange interaction compete with each other, resulting in intermediate coupling; however, increasing the f count from 6 to 7 shows a clear and pronounced shift in the power balance in favor of the exchange interaction, resulting in the large shift of the expectation value for the intermediate coupling curve in Fig. 1(b). The effect is in fact so strong that, compared to Am, not one but two electrons are transferred to the $f_{7/2}$ level in Cm (cf. Table I).

The spin and orbital magnetic moments, m_s and m_l, from atomic calculations are plotted against n_f in Fig. 2(a) and 2(b), respectively. In each graph, the three different angular-momentum coupling mechanisms are shown: LS, jj and intermediate. Examining the plots, we see that for some elements, the choice of coupling mechanism has a large influence on the spin and orbital moments. This is most remarkable for Cm ($n_f = 7$), where Fig. 2(a) shows that the spin moment is modest for the jj coupling limit, but is large for both LS and intermediate coupling. The fact that the spin moment for the intermediate coupling is almost as large as that for the LS limit is because the intermediate coupling curve moves strongly towards the LS limit at Cm in Fig. 1(b). It is the pronounced shift of the intermediate coupling curve towards the LS coupling limit at Cm—in order to accommodate the exchange interaction—that creates a large and abrupt change in the electron occupancy of the $f_{5/2}$ and $f_{7/2}$ levels shown in Fig. 2(c). In this figure, the $n_{5/2}$ and $n_{7/2}$ occupation numbers are shown for atomic calculations in intermediate coupling by the lines, and for the spin-orbit analysis of the experimental EELS spectra as points. The striking change in electron occupancy between Am and Cm is evident in this figure. If the intermediate coupling curve remained near the jj limit for Cm, the spin (and total) moment would be much smaller than the observed $7\mu_B$/atom [20] magnetic moment and have little or no effect on the crystal structure of the metal.

It is also interesting to compare Pu (f^5) and Cm (f^7). They both have roughly the same amount of $f_{5/2}$ electrons, but while Pu has 0.67 $f_{7/2}$ electrons, Cm has 2.59 (cf. Table I). The angular moment coupling of the five 5f electrons in Pu are governed by the strong spin-orbit interaction [13], resulting in a spin that is rigidly coupled antiparallel to its orbital moment. Figure 2(a) and 2(b) shows that for Pu, the spin and orbital magnetic moments are opposite and almost equal. Cm, however, has a small orbital moment that is aligned in the same direction as the large spin moment.

In order to progress from atomic to condensed matter, we have to use an appropriate computational method. The parameter-free DFT, which relies on the magnetic configuration, atomic number, and geometry as the only constraints, predicts accurate total energies for the actinide metals in general and can thus be utilized for predicting phase transitions. Here, magnetic interactions include spin and orbital polarization and spin-orbit coupling similar to
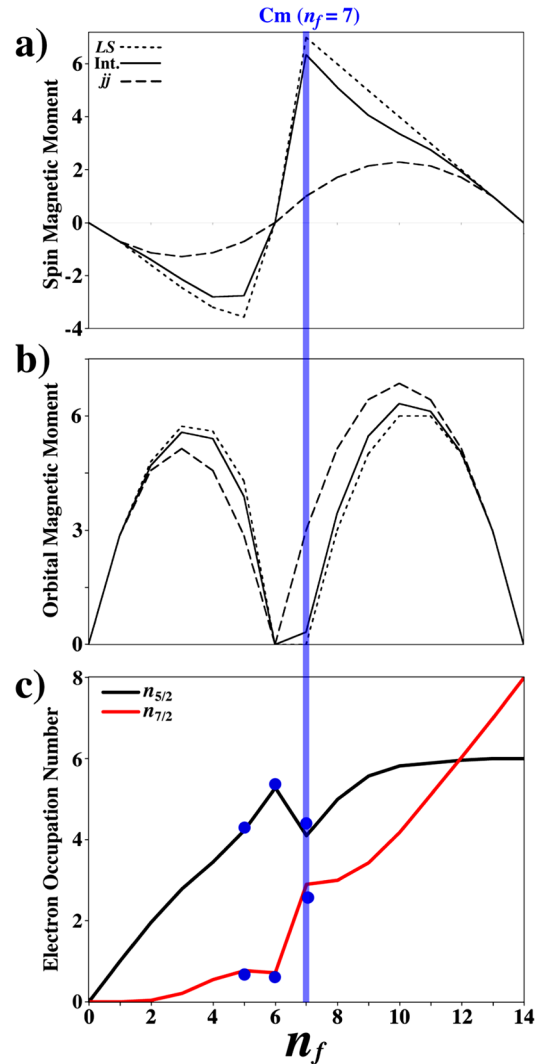
FIG. 2 (color online). The atomic (a) spin magnetic moment $m_s = -2\langle S_z \rangle = -2\sum_i s_{z,i}$ and (b) orbital magnetic moment $m_l = -\langle L_z \rangle = -\sum_i l_{z,i}$ (in μ_B) for the actinide elements against the number of 5f electrons (n_f). The total magnetic moment is $m_s + m_l$ (not shown). The three theoretical angular momentum coupling schemes in the many-electron configurations are shown in each plot: LS, jj, and intermediate coupling. (c) The electron occupation numbers $n_{5/2}$ and $n_{7/2}$ in intermediate coupling as a function of the n_f. The $n_{5/2}$ and $n_{7/2}$ occupation numbers from the spin-orbit analysis of the EELS spectra are indicated by points.

our calculations for Pu [10]. Nonmagnetic (NM) calculations presented below exclude these interactions. The total energies of the five polymorphic phases of Cm (I-V) are plotted as a function of volume in Fig. 3 for the NM and AF configuration (ferromagnetic order gives higher total energy for Cm). One conclusion is that spin polarization is needed to capture the correct order of phases, as previously shown [12]. What else is clear from Fig. 3 is that the NM calculations are much higher in energy than those including the magnetic interactions and that the NM-AF energy difference for Cm I, II and III is large, but becomes pro-
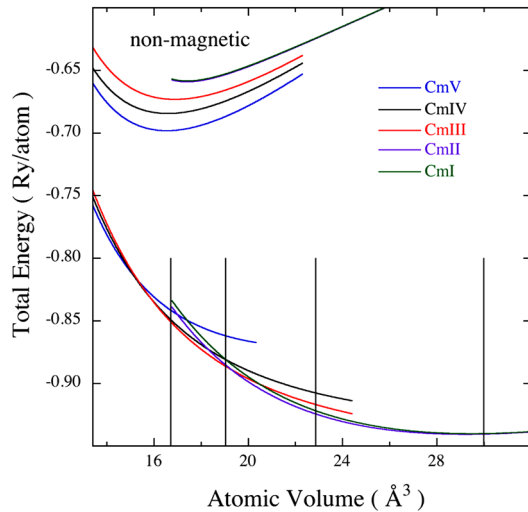
FIG. 3 (color online).   Total energies for the five polymorphic phases of Cm (I-V) as a function of atomic volume for AF and NM calculations. NM fcc and dhcp are nearly degenerate with less than 0.001 Ry difference throughout the entire volume range. Dhcp is lower than fcc at volumes above 28 Å^3. The vertical black lines indicate the experimentally measured phase transition volumes [12].

TABLE II.   The spin, orbital, and total moments, m_s, m_l and m_{total} (in μ_B) for Cm I-V as calculated by DFT.

Cm phase	Volume (Å^3)	m_s	m_l	m_{total}
I	30	6.6	0.4	7.0
II	22.8	6.16	0.35	6.51
III	18.9	5.43	0.38	5.81
IV	16.7	4.57	0.59	5.16
V	13.7	0	0	0

gressively smaller for Cm IV and V during compression. This means that magnetism is strong for the lower-pressure phases, but then diminishes, becoming less important for the high-pressure phases. As the volume is decreased, the 5f wave functions overlap increase, leading to broader bands that lessen the preference for spin and orbital polarization with reduced magnetism as a consequence. Indeed, examining the spin, orbital, and total magnetic moments in Table II, it can be seen that the moments steadily decrease with pressure.

Summarizing, in Cm the seven 5f electrons forming a half-filled shell are stabilized by exchange interaction, resulting in a large spin moment in both intermediate and LS coupling. This stabilization resembles that of Gd f^7, which has the highest Curie temperature amongst the rare earth elements and a large spin magnetic moment. Cm also has a modest orbital moment that is parallel to the large spin moment due to the nonvanishing spin-orbit interaction in intermediate coupling. Thus, it is clear why Cm is strongly magnetic, and here we see that the electron coupling mechanism plays a dominant role, being the root cause for the magnetic stabilization of curium. Our results mean that any computational model of the actinides must take into account the strong shift from jj to LS coupling from Am to Cm. Our experimental results are also in agreement with very recent dynamical mean field theory (DMFT) calculations for the actinide metals [21], which show the large change in spin-orbit expectation value between Am and Cm.

*Corresponding author
†Tel: 925-422-9741;
Fax: 925-422-6892;
moore78@llnl.gov

[1] P. Söderlind *et al.*, Nature (London) **374**, 524 (1995).
[2] O. K. Andersen *et al.*, Physica (Amsterdam) **86B+C**, 249 (1977).
[3] P. Söderlind *et al.*, Phys. Rev. B **50**, 5918 (1994).
[4] S. Y. Savrasov, G. Kotliar, and E. Abrahams, Nature (London) **410**, 793 (2001).
[5] L. Havela *et al.*, Phys. Rev. B **65**, 235118 (2002).
[6] J. L. Sarrao *et al.*, Nature (London) **420**, 297 (2002).
[7] G. H. Lander, Science **301**, 1057 (2003).
[8] J. Wong *et al.*, Science **301**, 1078 (2003).
[9] X. Dai *et al.*, Science **300**, 953 (2003).
[10] P. Söderlind and B. Sadigh, Phys. Rev. Lett. **92**, 185702 (2004); P. Söderlind, Europhys. Lett. **55**, 525 (2001).
[11] K. T. Moore *et al.*, Phys. Rev. Lett. **96**, 206402 (2006).
[12] S. Heathman *et al.*, Science **309**, 110 (2005).
[13] K. T. Moore *et al.*, Phys. Rev. Lett. **90**, 196404 (2003); K. T. Moore *et al.*, Philos. Mag. **84**, 1039 (2004); K. T. Moore *et al.*, Phys. Rev. B **73**, 033109 (2006).
[14] R. D. Cowan, *The Theory of Atomic Structure and Spectra* (University of California Press, Berkeley, 1981).
[15] G. van der Laan and B. T. Thole, Phys. Rev. B **53**, 14458 (1996).
[16] G. van der Laan *et al.*, Phys. Rev. Lett. **93**, 097401 (2004).
[17] P. Söderlind and A. Landa, Phys. Rev. B **72**, 024109 (2005).
[18] B. T. Thole and G. van der Laan, Phys. Rev. A **38**, 1943 (1988); Phys. Rev B **38**, 3158 (1988).
[19] *Handbook on the Physics and Chemistry of the Actinides*, edited by A. J. Freeman and G. H. Lander (Elsevier Science Ltd., Amsterdam, 1984).
[20] P. G. Huray *et al.*, Physica (Amsterdam) **102B+C**, 217 (1980); S. E. Nave, R. G. Haire, and P. G. Huray, Phys. Rev. B **28**, 2317 (1983).
[21] J. H. Shim, K. Haule, and G. Kotliar, Nature (London) **446**, 513 (2007).